Supporting Information

Supercapacitor-Based CO_2 Capture Enhanced by Electrolyte pH Control

Selina E. Wiesner[1,2], Zeke Coady[2], Zhen Xu[3], Malina Seyffertitz[2], and Alexander C. Forse[2]

[1] Faculty of Chemistry and Pharmacy, Ludwig-Maximilians-Universität München, Munich 81377, Germany.

[2] Yusuf Hamied Department of Chemistry, University of Cambridge, Cambridge CB2 1EW, United Kingdom.

[3] Department of Materials and Henry Royce Institute, University of Manchester, Oxford Rd, Manchester M13 9PL, United Kingdom

SI Figures

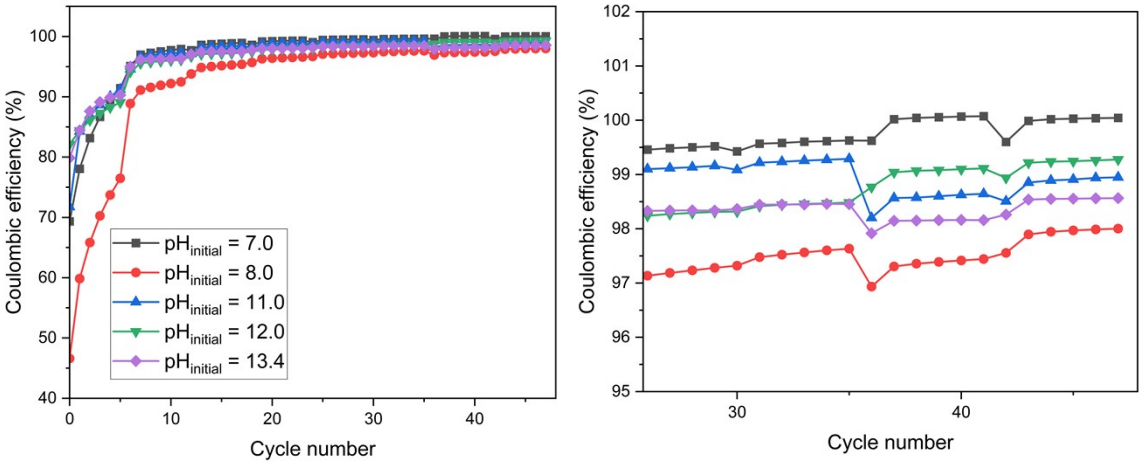

Figure S1: Coulombic efficiencies (CE, %) for 1 M Na_2SO_4 electrolytes with different pH_{inital}. a) CEs calculated as Discharge/ Charge capacity. **b)** Zoom in on CEs for higher cycle numbers. The low Coulombic efficiencies at low cycle numbers is explained by insufficient activation of the carbon electrolyte interface.

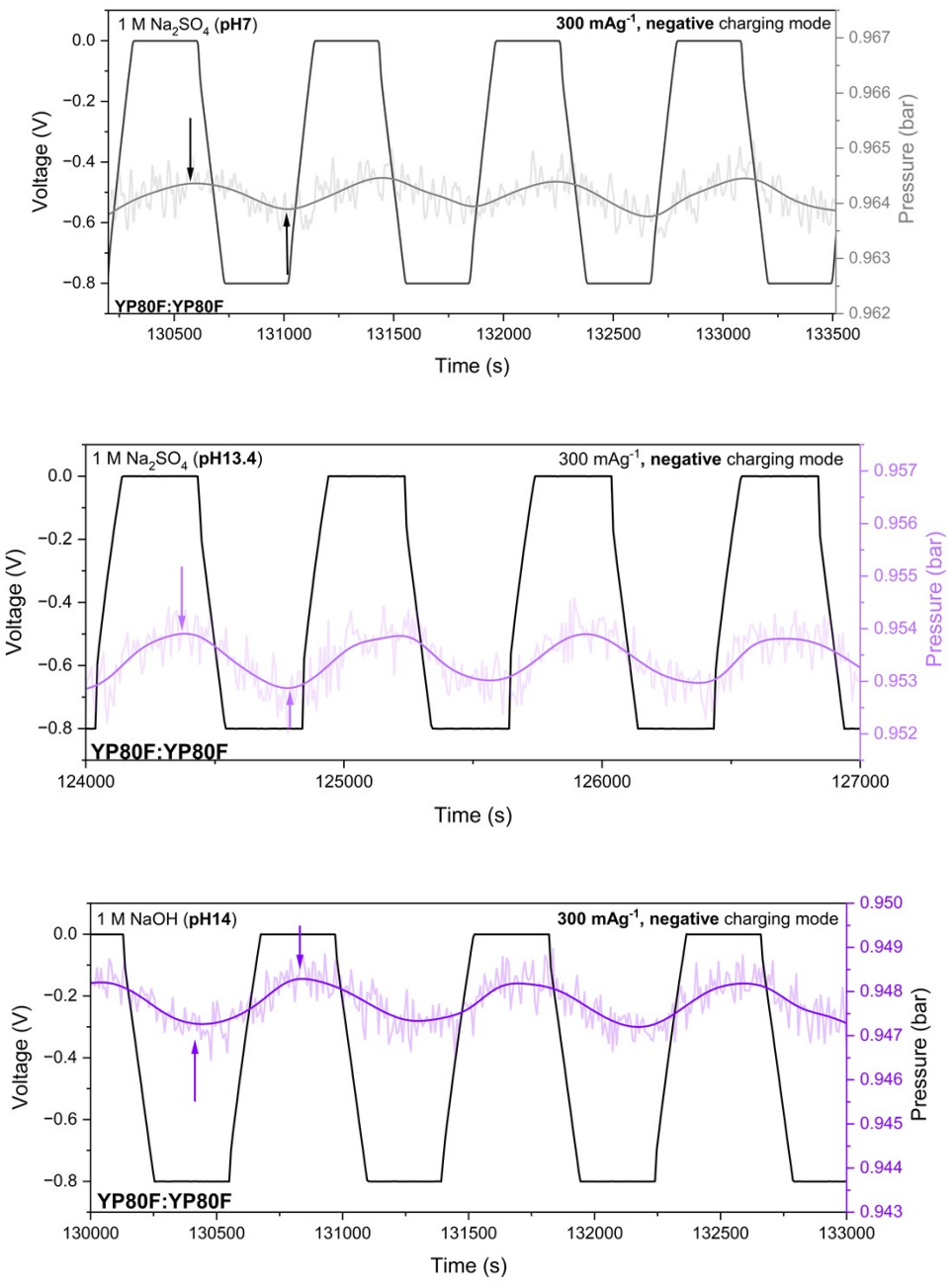

Figure S2: Pressure-voltage overview plots for the negative charging mode at 300 mAg^{-1}. The pressure curves oscillate within a defined pressure range, and the lack of an irreversible increase in pressure during charging suggests the absence of parasitic side reactions.

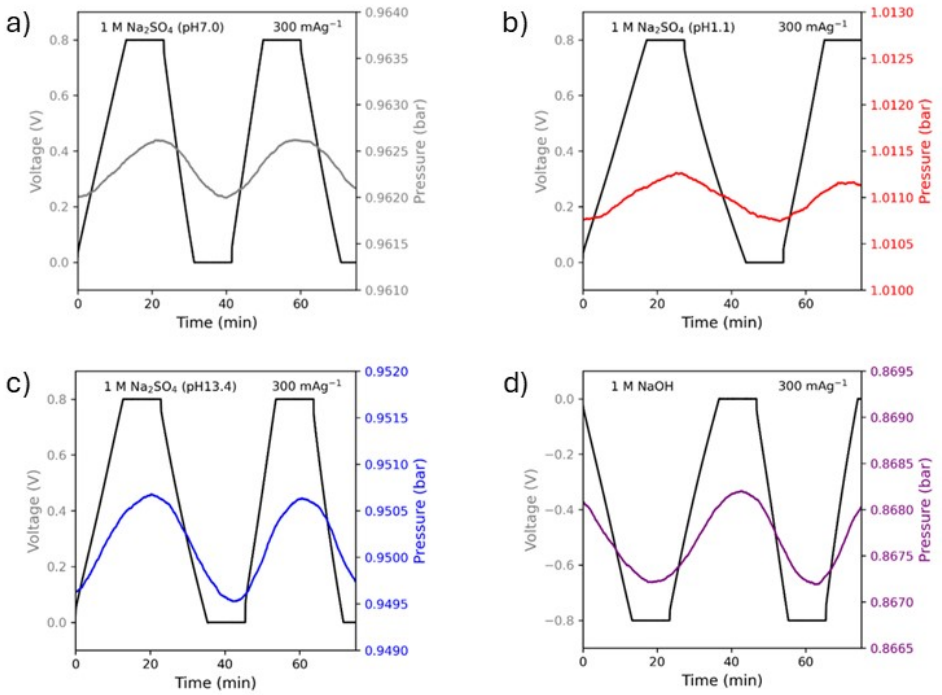

Figure S3: Pressure voltage curves for different electrolyte pH in the positive charging mode, for supercapacitor cells with YP80F electrodes, with pure CO_2 gas the cell headspace. When the supercapacitor cells are charged positively, CO_2 release is observed during charging (evidenced by the increase in pressure). All cells are charged to + 0.8 V and are discharged after a 5-min voltage hold. **a)** Neutral (pH initial 7.0) Na_2SO_4 electrolyte. **b)** Acidic (pH initial 1.1) Na_2SO_4 electrolyte. **c)** Basic (pH initial 13.4) Na_2SO_4 electrolyte. **d)** 1 M NaOH (pH initial 14.0).

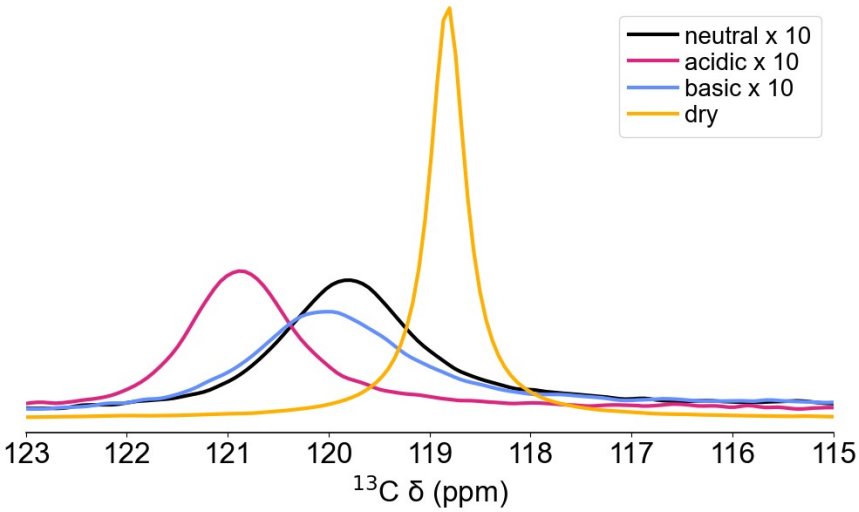

Figure S4: Comparison of the in-pore CO_2 peak observed after $^{13}CO_{2(g)}$ dosing in the ^{13}C ss-NMR (9.4 T, 5 kHz MAS) spectra of the *neutral* electrolyte/electrode system (Figure 2e), the *acidic* electrolyte/electrode system (Figure 2f), the *basic* electrolyte/electrode system (Figure 2g), and a dry

YP80F electrode sample. In the dry electrode system, reflecting $CO_{2(g)}$ uptake, this peak possesses a notably different chemical shift, linewidth, and peak integration than the electrolyte/electrode systems, reflecting the change in phase between these systems.

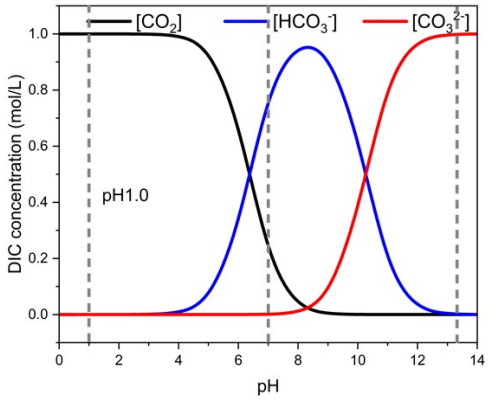

Figure S5: Bjerrum Plot showing the theoretical speciation of CO_2-derived species for pure water depending on pH (without activated carbon present). Plot derived with equilibrium constants from Millero et al.[1]

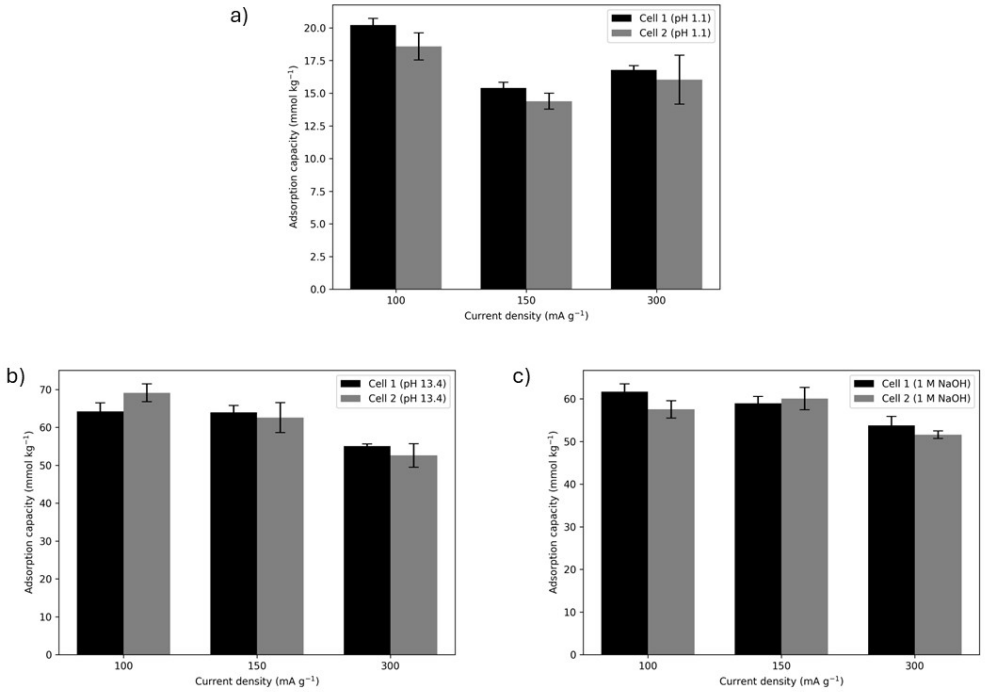

Figure S6: Reproducibility of adsorption capacities for coin cells. Two individual coin cell type supercapacitors (Cell A and Cell B) were assembled on different days by the same researcher and measured in two different gas cells (**Figure 2a**, main text) to ensure reproducibility. The deviations between Cell A and Cell B are within the error bar (calculated for 5 repetitions measured for the individual coin cell) a) Acidic Na_2SO_4 (pH initial 1.1) electrolyte b) basic Na_2SO_4 (pH initial 13.4) electrolyte c) 1 M NaOH electrolyte.

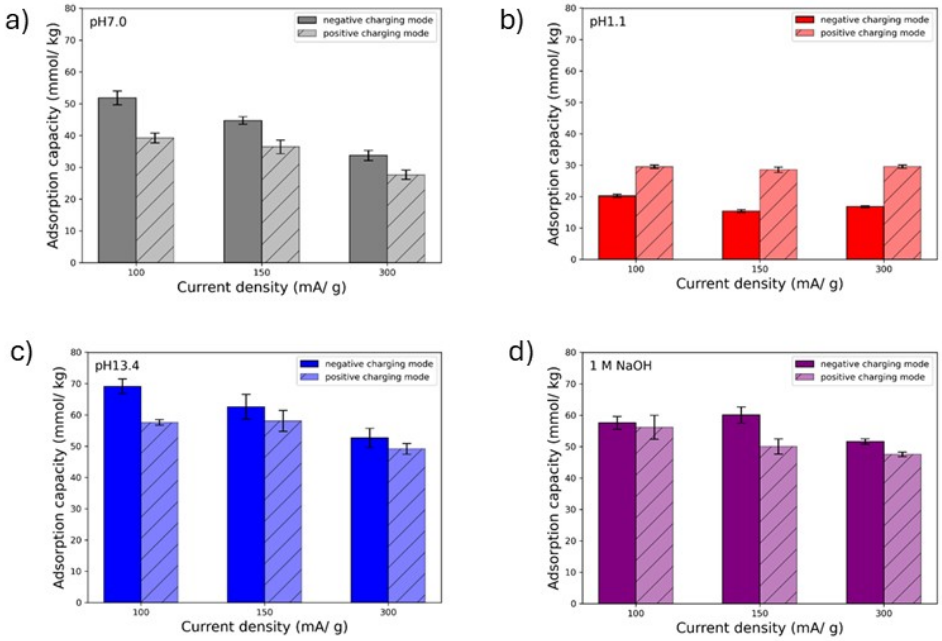

Figure S7: Comparison of CO_2 adsorption capacities (mmol/ kg) in the negative and positive charging mode for different pH electrolytes. **a)** Neutral (pH initial 7.0) Na_2SO_4 electrolyte. **b)** Acidic (pH initial 1.1) Na_2SO_4 electrolyte. **c)** Basic (pH initial 13.4) Na_2SO_4 electrolyte. **d)** 1 M NaOH (pH initial 14.0).

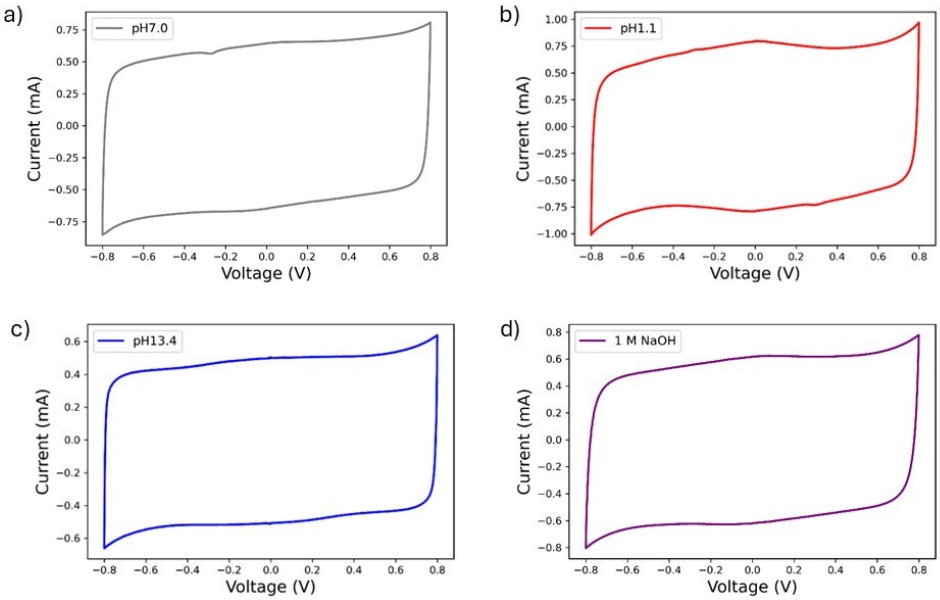

Figure S8: Cyclic voltammetry curves measured under CO_2 atmosphere for different electrolyte pH. **a)** Neutral (pH initial 7.0) Na_2SO_4 electrolyte. **b)** Acidic (pH initial 1.1) Na_2SO_4 electrolyte. **c)** Basic (pH initial 13.4) Na_2SO_4 electrolyte. **d)** 1 M NaOH (pH initial 14.0).

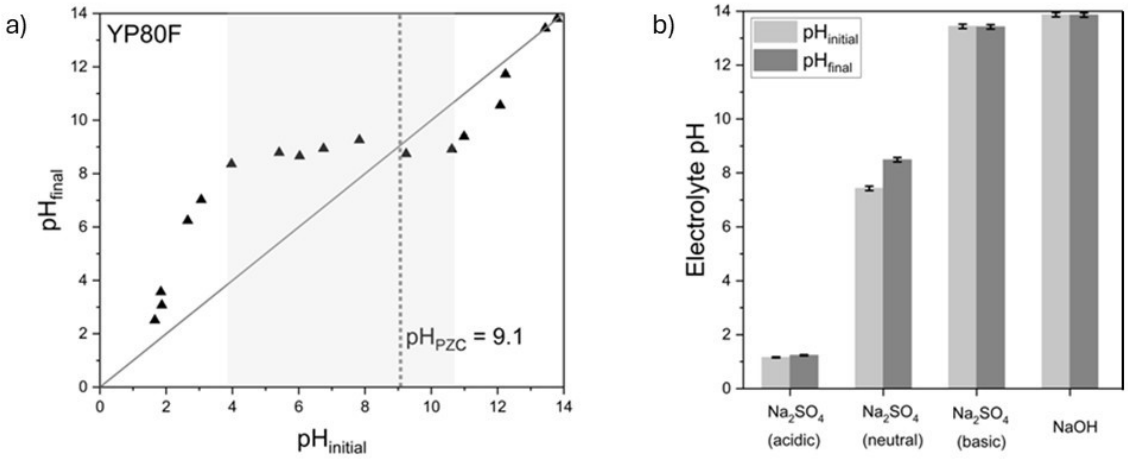

Figure S9: Interaction of carbon electrode (YP80F) with the electrolyte. **a)** Point of zero charge (PZC) of YP80F thin film measured under air after 24h equilibration time. PZC was determined using Na_2SO_4 electrolyte with the pH adjusted using NaOH for the basic range and H_2SO_4 for the acidic range of the pH scale. The mass ratio between carbon and electrolyte is the same as that within meshed coin cells. pH_{PZC}(YP80F) = 9.1. **b)** pH_{final} measurements for the acidic, neutral, basic Na_2SO_4 electrolyte and for the 1 M NaOH under air. Experiment was performed analogously to a) using YP80F thin film material and a pH-adjusted Na_2SO_4 electrolyte. pH of acidic and basic electrolytes and NaOH is not significantly influenced by proton uptake from the electrolyte as $pH_{initial}$ and pH_{final} do not deviate a lot from each other.

Table 1: pH_{finals} extracted from de-crimped coin cells.

Electrolyte name	**Acidic Na_2SO_4**	**Neutral Na_2SO_4**	**Basic Na_2SO_4**	**NaOH**
$pH_{initial}$	1.1	7.0	13.4	14.0
pH_{final}	1.3	8.4	9.6	12.3

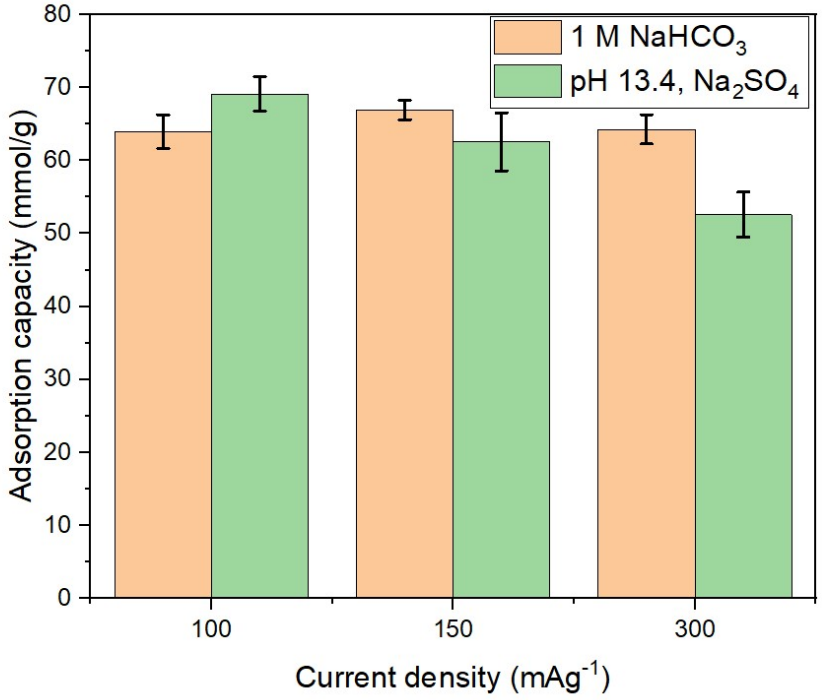

S10: Comparison of negative charging mode using 1 M $NaHCO_3$ and using 1 M Na2SO4 (pH 13.4) as an electrolyte.

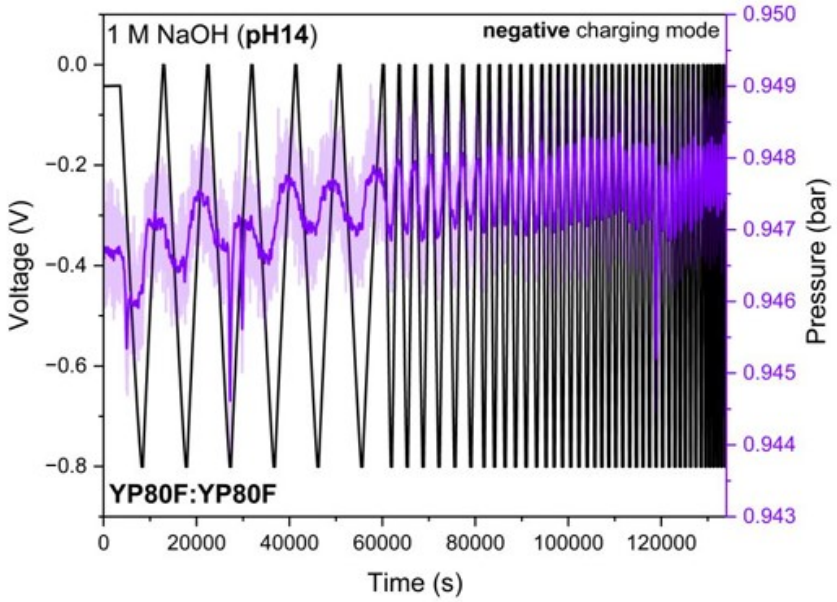

S11: Continuous pressure change in basic electrolyte attributed to corrosion with longer measurement times (36 h). Local spikes in pressure come from opening and closing of the incubator oven during the ongoing measurement.

SI Calculations

Electrochemical Gas Cell Calculations

Specific CO_2 adsorption capacities

For the calculation of the specific CO_2 adsorption capacity (CCO_2, mmol kg^{-1}) the amount of gas adsorbed was obtained from the difference in pressure using the ideal gas law in Equation 1:

$$n = \frac{pV}{RT} \qquad (1)$$

with n the gas amount (mol), p pressure (Pa, 10^{-5} bar), V volume (m^3, 10^6 mL), T the temperature (K) and R the ideal gas constant (R = 8.31451 m^3 Pa mol^{-1} K^{-1}). To compensate for the slight irreversible decrease in the overall pressure curve arising from side reactions, an average of two maximum points is used as shown in Equation 2:

$$\Delta n = \frac{(n_{max1} + n_{max2})/2}{n_{min}} \qquad (2)$$

where n_{max1} and n_{max2} represent the two maxima peaks of the gas amount adsorbed and n_{min} represents the minimum peak of the pressure curve.

The volume of the gas reservoir V_1 (mol) in each gas cell was calculated prior to every gas adsorption measurement during a pressure test according to Boyle's Law (Equation 3).

$$p_1 V_1 = p_2 V_2 \qquad (3)$$

For each individual gas cell, the volume in a section between two valves is known from calibration (A mL). For the dosing, the gas between two valves was removed first by applying a vacuum. The gas amount in the main gas reservoir is proportional to $p_1 V_1$, where p_1 is shown by the pressure sensor. After evacuation, CO_2 is dosed into the evacuated portion of the known volume (A mL). The total amount of gas remained the same, but as the pressure decreased to p_2 (bar) the volume of the reservoir (V_1 , mL) was calculated using Equation 4:

$$V_1 = \frac{p_2 A}{p_1 - p_2} \qquad (4)$$

This step also fulfils as a leaking test to make sure that the coin cell was assembled tightly and that there is no leaking within the gas cell.

With Equation 5, the CO_2 adsorption capacity C_{CO_2} (mmol kg^{-1}) which is normalized to the active mass of the electrodes are calculated. The errors of the overall adsorption capacities were calculated using a 95% confidence interval with the Students t-test.

$$C_{CO_2} = \frac{\Delta n}{m} \times 10^6 \qquad (5)$$

Adsorption rates

The CO_2 adsorption rates (R_{CO2}, $mmol_{CO2}$ kg^{-1} h^{-1}) were calculated using Equation 6:

$$R_{CO2} = \frac{C_{CO2}}{t_{charging}/3600} \qquad (6)$$

where C_{CO2} is the measured CO_2 adsorption capacity and $t_{charging}$ corresponds to the total charging time (including the voltage hold step).

Gravimetric capacitance

The specific discharge capacitance values ($C_{electrode}$, F g^{-1}) of the working electrodes were calculated from the GCD data according to Equation 7:

$$C_{electrode} = 2\frac{I\,\Delta t}{m\,\Delta U} \qquad (7)$$

with $C_{electrode}$ (F g^{-1}) as the specific discharge capacitance of the working electrode, I (A) as the constant discharge current, ΔU (V) as the cell voltage, m (g) as the mass of the active electrode material (95% of the absolute electrode mass) and Δt (s) as the charge/ discharge time.

The cell voltage ΔU (V) is calculated from the discharge curve of the GCD data using Equation 8:

$$\Delta U = U_{max} - IR_{drop} - U_{min} \qquad (8)$$

Quantitative ss-NMR Calculations

Measurements were performed under quantitative conditions for the CO_2 and HCO_3^- peaks, with D_1 delay times set to > 5 * T_1 for each of these peaks, with T_1 measured by inversion recovery experiments.

The spectra also include contributions from ^{13}C in the unenriched activated carbon. A broad background peak is observed centred at approximately 120 ppm, along with a spinning sideband at approximately 170 ppm. These were assigned based on ^{13}C measurements of the dry activated carbon (Figure **S8**) in alignment with literature measurements.[2–4]

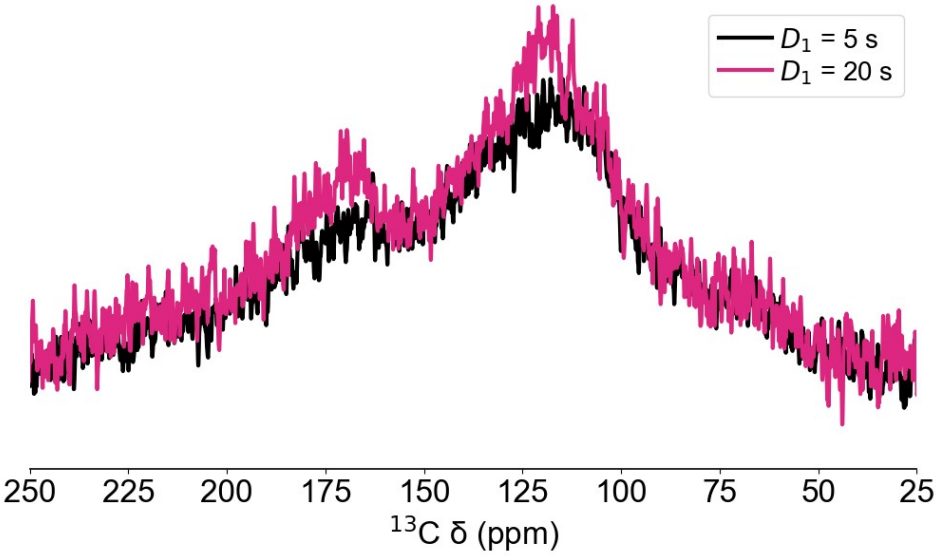

Figure S12: ^{13}C NMR of dry, undosed YP80F film, measured with D_1 delay times of 5 s (as was used for the NMR experiments on dosed samples in Figures 2 and 4) and 20 s (to better display the peaks at 120 and 170 ppm).

The contribution of these background resonances to the integrations of the $^{13}CO_2$-dosed systems was removed by subtraction of a ^{13}C spectrum of the undosed YP80F film after processing. The spectrum of the undosed YP80F film was scaled to the mass of the carbon and the number of scans of the original system, and was recorded with an identical D_1 to the measurements of the $^{13}CO_2$-dosed systems.

In order to relate the peak integration of our quantitative NMR experiments (I_{CO_2} and $I_{HCO_3^-}$) to the initial gravimetric uptake of CO_2 and HCO_3^- ($C^{in}_{CO_2}$ and $C^{in}_{HCO_3^-}$), NMR integrations were

referenced to CO_2 uptake in dry activated carbon. This was performed following an identical procedure as the one described previously.[5] C^{in} values were then calculated using Equation 9:

$$C^{in} = \frac{I}{10^{11}} \times a + b \qquad (9)$$

a relates integration to moles of CO_2, and a value of 0.4361 mmol g^{-1} was calculated from calibration. b was included to account for remaining baseline distortion after background correction, and a value of 0.01995 mmol g^{-1} was calculated from calibration. Using this referencing process corrects for potential signal attenuation caused by the skin depth effect.[6–8]

References

(1) Millero, F. J.; Graham, T. B.; Huang, F.; Bustos-Serrano, H.; Pierrot, D. Dissociation Constants of Carbonic Acid in Seawater as a Function of Salinity and Temperature. *Mar. Chem.* **2006**, *100* (1–2), 80–94. https://doi.org/10.1016/j.marchem.2005.12.001.

(2) Puziy, A. M.; Poddubnaya, O. I.; Socha, R. P.; Gurgul, J.; Wisniewski, M. XPS and NMR Studies of Phosphoric Acid Activated Carbons. *Carbon* **2008**, *46* (15), 2113–2123. https://doi.org/10.1016/j.carbon.2008.09.010.

(3) Freitas, J. C. C.; Emmerich, F. G.; Cernicchiaro, G. R. C.; Sampaio, L. C.; Bonagamba, T. J. Magnetic Susceptibility Effects on 13C MAS NMR Spectra of Carbon Materials and Graphite. *Solid State Nucl. Magn. Reson.* **2001**, *20* (1–2), 61–73. https://doi.org/10.1006/snmr.2001.0030.

(4) Freitas, J. C. C.; Bonagamba, T. J.; Emmerich, F. G. Investigation of Biomass- and Polymer-Based Carbon Materials Using 13C High-Resolution Solid-State NMR. *Carbon* **2001**, *39* (4), 535–545. https://doi.org/10.1016/S0008-6223(00)00169-X.

(5) Coady, Z.; Brookes, S.; Shen, Z.; Rhodes, B.; Mapstone, G.; Xu, Z.; Yu, W.; Nishihara, H.; Schran, C.; Michaelides, A.; Forse, A. Unexpected Oversolubility of CO2 Measured at Electrode-Electrolyte Interfaces. ChemRxiv June 12, 2025. https://doi.org/10.26434/chemrxiv-2025-r7jr6.

(6) Mincey, D. W.; Popovich, M. J.; Faustino, P. J.; Hurst, M. M.; Caruso, J. A. Monitoring of Electrochemical Reactions by Nuclear Magnetic Resonance Spectrometry. *Anal. Chem.* **1990**, *62* (11), 1197–1200. https://doi.org/10.1021/ac00210a020.

(7) Bhattacharyya, R.; Key, B.; Chen, H.; Best, A. S.; Hollenkamp, A. F.; Grey, C. P. In Situ NMR Observation of the Formation of Metallic Lithium Microstructures in Lithium Batteries. *Nat. Mater.* **2010**, *9* (6), 504–510. https://doi.org/10.1038/nmat2764.

(8) Ilott, A. J.; Chandrashekar, S.; Klöckner, A.; Chang, H. J.; Trease, N. M.; Grey, C. P.; Greengard, L.; Jerschow, A. Visualizing Skin Effects in Conductors with MRI: (7)Li MRI Experiments and Calculations. *J. Magn. Reson. San Diego Calif 1997* **2014**, *245*, 143–149. https://doi.org/10.1016/j.jmr.2014.06.013.